Ionic interactions in platinum chloride linear-chain compounds

I. Batistić
Institute of Physics of the University, P.O. Box 304, 41001 Zagreb, Croatia

X. Z. Huang, A. R. Bishop, and A. Saxena
Theoretical Division, Los Alamos National Laboratory, Los Alamos, New Mexico 87545
(Received 16 February 1993; revised manuscript received 30 April 1993)

Halogen-bridged transition-metal chain compounds have recently emerged as an important class of low-dimensional electronic materials with strong electron-lattice and electron-electron interactions. We introduce a many-body model for such materials which is quantitatively successful for highly valence-localized (strong charge-density-wave) members of the class, e.g., PtCl with various ligand structures. The model introduces nearest-neighbor Coulomb attraction *and* metal ion-ion electrostatic repulsion directly rather than through a linear Peierls-Hubbard Hamiltonian. These interactions have the effects of (i) modifying the on-site orbital energies, (ii) generating an effective *anharmonic intra*site electron-lattice coupling (leading to the formation of a charge-density-wave even if the intersite electron-lattice coupling is weak), and (iii) acting as an effective *anharmonic* elastic force between neighboring metal and halogen atoms. The stoichiometric ground state and various defect states (polaron, bipolaron, kink, exciton) are studied within this framework by computing their optical absorption, Raman, and infrared spectra: The results agree well with available experimental data. Buckling of Cl atoms out of the chain axis in certain PtCl compounds is predicted to be important in order to obtain the observed Raman frequencies for *electron* polarons and bipolarons. Finally, a strong "template" effect is discussed by comparing two PtCl materials with different ligands and counterions.

I. INTRODUCTION

The chemical and physical properties of low-dimensional, molecular solids have been the subject of intense study in recent years, both because of the intrinsically interesting properties of the materials and because of their potentially important technological applications. These materials have in common both low dimensionality and competing electron-phonon (e-ph) and electron-electron (e-e) interactions, leading to a variety of broken-symmetry ground states (e.g., charge- and spin-density waves, superconductivity) and related mesoscopic ordering. Examples of such materials are the high-temperature superconductors, organic superconductors, conducting polymers, charge-transfer salts, charge-density-wave materials, and the materials discussed here, halogen-bridged mixed-valence transition-metal linear-chain complexes, hereafter referred to as MX chain compounds; see Refs. 1–5 for extensive discussions of MX materials.

Certain MX chain compounds have been of interest to chemists for many decades as strongly dichroic materials.[1] A typical crystal consists of an array of linear chains of alternating metal (M) and halogen (X) atoms; with ligands attached to the metals, and in some cases counterions between the chains to maintain charge neutrality. Symbolically, the MX complex can be represented by $[M^{\rho-\delta}L_4][M^{\rho+\delta}X_2L_4]Y_4$, where X is Cl, Br, I; M is Pt, Pd, or Ni; and δ denotes the deviation of the valence of the transition-metal ions from the average valence ρ; L is a ligand molecule such as X, ethylamine, ethylenediamine (L_2), or cyclohexanediamine (L_2); and Y is a counterion such as X or ClO_4^-, present if the chains are not neutral. In the ground state of the Ni materials there is no (or extremely weak) observed charge disproportionation ($\delta \simeq 0$) or lattice distortion. In the ground state of typical Pt and Pd materials, the strong valence dimerization of the M sublattice is stabilized by a similarly strong dimerization of the X sublattice displacement. In other words, the X atoms are displaced from the midpoint between neighboring M atoms, giving rise to charge disproportionation (mixed valence) on the M atoms, e.g., Pt^{II} or Pt^{IV} instead of the average Pt^{III}. Some examples include the ethylenediamine (en) complexes, $[Pt(en)_2][Pt(en)_2X_2](ClO_4)_4$, hereafter referred to as PtX (X = Pt, Br, I). The structure of the PtCl complex, shown in Fig. 1, is representative of the MX class. The major differences between members of the class are (i) the extent of lattice distortion, with PtCl, PtBr, and PtI typical of MX chains ranging from strongly to weakly distorted limits, and (ii) whether the chains are charged, as in the above examples (with Y=ClO_4^-), or neutral, as is the case for $[Pt(NH_3)_2Br_2][Pt(NH_3)_2Br_4]$.

Microscopic modeling of strongly correlated electronic materials such as the MX class or those others listed earlier has the aim of utilizing a minimal many-body Hamiltonian which focuses on the essential electronic orbitals and lattice degrees of freedom needed to explain ground-state and excited-state properties. Ideally, input for the model many-body Hamiltonian parameters is taken from

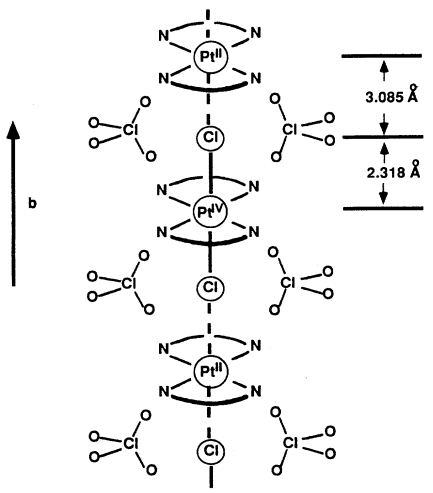

FIG. 1. Structure of the PtX materials, $[Pt(en)_2][Pt(en)_2Cl_2](ClO_4)_4$, obtained by x-ray diffraction [S.C. Huckett (unpublished)].

ab initio calculations and then numerical or analytical techniques are applied to the many-body Hamiltonian to predict experimentally measurable quantities (optical absorption, phonon spectroscopy, etc.). In reality, few complex materials have permitted closure of this iterative modeling strategy. The MX class, however, is proving an exception, and therefore is an important *class* of materials from the point of view of many-body modeling strategies for complex electronic systems more generally. In particular, we have introduced earlier[4] an extended two-band Peierls-Hubbard one-dimensional model. This has been able to describe successfully much of the systematic structural, electronic, and phonon properties not only in the stoichiometric (homogeneous) ground states but also (using the *same* model parameters) for a variety of intrinsic defect states induced by chemical or photo doping—namely, solitons, polarons, bipolarons, and excitons. This model has proved to be widely successful in that it gives a good account of systematic variations in properties of all PtX materials, as well as the experimentally observed segment length dependence of the resonant Raman modes for the mixed-halide $PtBr_xCl_{1-x}$ (Ref. 5) and PtI_xCl_{1-x} (Ref. 6) compounds. It also predicts an observed photo-induced charge-transfer effect in $PtBr_xCl_{1-x}$,[7] and can explain variations in ESR spectra.[8]

An exception to the above near-quantitatively modeled materials are the very *valence-localized* MX examples such as the PtCl family. In these cases, the stoichiometric materials are described quantitatively,[4] but the defect states cannot be predicted satisfactorily with the same Hamiltonian parameters for *both* electronic and phonon properties. We propose here that the reason is the strongly ionic limit of these members of the MX class (analogous to a "one-dimensional NaCl" ionic crystal and color centers therein). In this regime our earlier[4] model assumptions of a *linear* spring constant and electron-lattice interactions, although typical of current literature for Peierls-distorted materials, are inadequate to describe the effects of large charge redistributions around spatially localized defect states. The fact that PtCl compounds have large Peierls' distortions (e.g., 10% of the lattice constant) already suggests the possibility of anharmonic effects. One major consequence is the large shift of Raman phonon frequencies for polaron excitations, relative to the homogeneous stoichiometric material's Raman frequency. These considerations lead us to return here to a more fundamental description of the anharmonic effects in PtCl, in terms of explicit Coulomb attraction and electrostatic repulsion forces.[9] Since the linear approximation is so widely used in Peierls-Hubbard modeling of whole classes of novel electronic materials (above), this lesson for PtCl has wider significance than the specific examples discussed here.

In valence-*delocalized* materials (e.g., PtBr, PtI), our generalized description is equivalent to our previous linear Peierls-Hubbard tight-binding model (see the Appendix). However, for the ionic limit, there are minimal band screening effects, so that a linear spring constant between neighboring Pt and X is insensitive to the local charge environment. Then local Raman modes associated with defect states (polarons, excitons, bipolarons, etc.) are hardly changed in frequency from the homogeneous chain:[10] This is contrary to experimental data—e.g., for $[Pt_2(en)_4Cl_2](ClO_4)_4$ Raman frequencies for electron and hole polarons are assigned at 263 cm^{-1} and 287 cm^{-1}, respectively,[11] compared with the uniform chain Raman frequency of 311 cm^{-1}.

As pointed out by Bulou *et al.*,[12] because of the significantly changed local charge distribution, the polaron states of PtCl are associated with locally changed effective elastic constants (i.e., in a pure lattice dynamical model), different from that of a uniform chain. Using pure lattice dynamics for a small chain segment, and assuming an exponentially decaying electrostatic repulsive force between neighboring Pt and Cl atoms, these authors calculated the elastic constants of various defect states by fitting the Raman frequencies. However, this approach is unable to determine electronic properties (e.g., optical absorption), and to impose self-consistency between the electronic and vibrational fields.

To address these self-consistency issues, we extend our previous model by *not* assuming a harmonic nearest-neighbor spring constant, but introducing instead an ion-ion *repulsive* force plus the Coulomb *attraction* between neighboring Pt and Cl atoms. As we will see, this leads to effectively *anharmonic* elastic and electron-lattice interactions—corresponding to modifications of the frequently used extended linear Peierls-Hubbard model. These modifications are essential for *quantitative* modeling of polaronic defects in strongly ionic materials. We first determine the model parameters by fitting the ground-state data (dimerization, electronic absorption, Raman), and then use the *same* set of parameters to accurately predict the Raman frequencies (as well as electronic properties) of various defect states. We will also see that a *buckling* of Cl atoms out of the axis of the chain around the electronic defect is necessary to achieve the observed relative ordering of Raman frequencies for electron and hole polarons (and bipolarons).

Another important consideration is the issue of a recently observed "template" effect.[13] Namely, the MX family exhibits a very large tunability in electronic properties by changing not only M and X, but also the ligand and counterion, which control mean chain lattice constants, i.e., acting as an effective internal pressure. To illustrate this effect, we will show below that two PtCl materials, $[Pt_2(en)_4Cl_2](ClO_4)_4$ and $[Pt_2(chxn)_4Cl_2]Cl_4$ (see below for meanings of ligands en and chxn), have quite different charge-density-wave strengths, reflected in their corresponding ratio of long and short Pt-Cl bond lengths, intervalence charge-transfer (IVCT) energy gaps, and Raman phonon frequencies.

This paper is organized as follows: In Sec. II, our model Hamiltonian is presented; in Sec. III, parameters are chosen to fit the ground-state properties for the two PtCl materials, and the template effect is briefly discussed; in Sec. IV, using the parameters found in Sec. III, various polaronic defect states are studied, including the difference between electron and hole polarons in terms of the presence and absence of buckling, respectively. Finally, Sec. V contains concluding comments.

II. MODEL

Based on the ideas in Sec. I, we use the following Hamiltonian for a single MX chain (with effective parameters in a three-dimensional MX environment):

$$H = \sum_{i,\sigma}\{[-t_0 + \alpha(x_{i+1} - x_i)](c^\dagger_{i,\sigma}c_{i+1,\sigma} + c^\dagger_{i+1,\sigma}c_{i,\sigma}) + e_i n_{i,\sigma}\} + \sum_i U_i n_{i,\uparrow}n_{i,\downarrow} + \sum_{i,\sigma} V_c \frac{(n_{i,\sigma} - Z_i)(n_{i+1,\sigma} - Z_{i+1})}{R_{i,i+1}} + \sum_i \frac{\mu}{R^\nu_{i,i+1}} + \sum_i \left(\frac{p_i^2}{2M_i} + \frac{1}{2}K_i(x_{i+1} - x_{i-1})^2\right). \quad (1)$$

Here, $c^\dagger_i$ and c_i are the electron creation and annihilation operators at site i with spin σ, and $n_{i\sigma}$ is the corresponding number operator (i refers to both M and X sites). t_0, α, e_i, U_i are the electron transfer integral, *inter*site electron-lattice coupling, on-site energy ($= e_0$ for Pt and $-e_0$ for Cl), and on-site Coulomb (Hubbard) strengths (U_M and U_X), respectively, and a is the average Pt-Cl bond length. x_i is the position of the ith atom, and p_i is its conjugate momentum. The distance between two neighboring atoms, with both parallel (x) and perpendicular (y) to the chain directions being included to allow for the possibility of buckling is

$$R_{i,i+1} = \sqrt{(x_{i+1} - x_i + a)^2 + (y_{i+1} - y_i)^2}. \quad (2)$$

As will be seen below, y_i are predicted to be zero for ground, hole polaron (bipolaron), and exciton states.

Compared with our previous model, the Hamiltonian (1) omits two terms (see Ref. 4 for notation): the uniform spring constant, K_{MX}, term (we still keep the second-nearest-neighbor K_i term which, for simplicity, we take nonzero only for K_{MM}) and the *intra*site electron-lattice coupling, β, term. Instead, we have explicitly included a nearest-neighbor Coulomb term in (1):

$$V_c \frac{(n_i - Z_i)(n_{i+1} - Z_{i+1})}{x_{i+1} - x_i + a}, \quad (3)$$

and an electrostatic repulsion term with power-law dependence (other model dependencies are equally acceptable):

$$\frac{\mu}{(x_{i+1} - x_i + a)^\nu}. \quad (4)$$

The structure of a single MX chain, including the possible buckling of X atoms, and associated model parameters is shown schematically in Fig. 2. In the Coulomb term, Eq. (3), Z_i is the positive ion charge at site i (i.e., excluding the valence shell described by n_i) , which is $Z_M = 4$ for Pt and $Z_X = 1$ for Cl. Since PtCl is very valence localized, n_{Cl} is always near 2, and n_{Pt} is always near 2 for Pt^{II} (reduced Pt) and to 0 for Pt^{IV} (oxidized Pt). Therefore, the numerator in the Coulomb term is always negative, yielding an attractive interaction. We also note that this term, proportional to V_c, is the *bare* nearest-neighbor Coulomb interaction. Consequently, there is an upper limit for the parameter V_c, namely 14.416 eV Å, i.e., the unscreened Coulomb energy for two-point unit charges separated by 1 Å.

The Hamiltonian (1) is to be solved self-consistently with the equation minimizing the total energy with respect to ion positions in an adiabatic sense.[4] The equa-

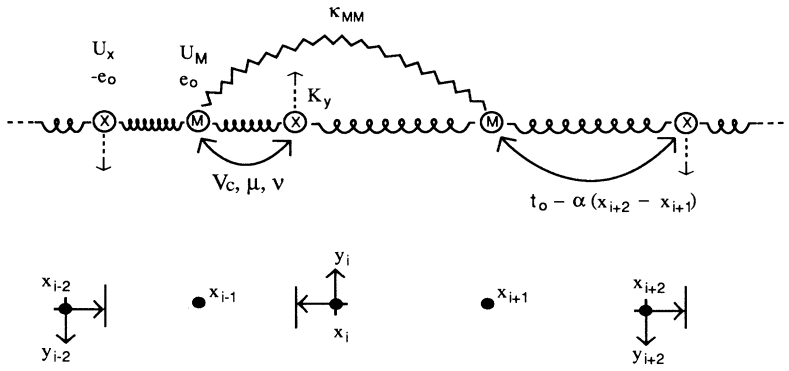

FIG. 2. Schematic of the MX chain showing the model parameters, buckling of X atoms, and a CDW distortion (see text for notations).

tion minimizing energy is determined by taking the first derivatives of the total energy from the Hamiltonian (1) with respect to each x_i and equating these equations to zero. The total energy from (1) includes elastic and electronic contributions and is determined by diagonalizing the electronic components for a given distribution of ion positions x_i. The electron-electron interactions are treated in a mean-field approximation (MFA).[4] In the case of the homogeneous (stoichiometric) chain, there is no buckling, and the equation minimizing the energy is

$$\frac{\mu\nu}{(x_{i+1}-x_i+a)^{\nu+1}}+V_c\frac{(n_i-Z_i)(n_{i+1}-Z_{i+1})}{(x_{i+1}-x_i+a)^2}-2\alpha\langle c_{i+1}^{\dagger}c_i\rangle+K_{i-1}(x_i-x_{i-2})$$

$$-\frac{\mu\nu}{(x_i-x_{i-1}+a)^{\nu+1}}-V_c\frac{(n_i-Z_i)(n_{i-1}-Z_{i-1})}{(x_i-x_{i-1}+a)^2}+2\alpha\langle c_i^{\dagger}c_{i-1}\rangle-K_{i+1}(x_{i+2}-x_i)=0\ . \quad (5)$$

Equation (5) constitutes a set of N (the number of chain sites) coupled nonlinear equations. This set of equations is also valid in the hole doping (inhomogeneous) case where no buckling of the chain is predicted.

For the stoichiometric case, the lowest-energy self-consistent solutions are the dimerized lattice–charge-density-wave ground states described in Sec. I. Introducing a_l and a_s as the long and short Pt–Cl bond lengths in such a dimerized ground state, and t_1 and t_2 as the corresponding electron transfer integrals between neighboring Pt and Cl atoms for the long and short Pt–Cl bonds, respectively,

$$t_1=\alpha\langle c_{\mathrm{Pt^{II}}}^{\dagger}c_{\mathrm{Cl}}\rangle+\text{c.c.}\ , \quad (6)$$

$$t_2=\alpha\langle c_{\mathrm{Pt^{IV}}}^{\dagger}c_{\mathrm{Cl}}\rangle+\text{c.c.}\ , \quad (7)$$

and the total Pt or Cl charge expectation values defined as [see Eq. (3)]

$$\rho_1=\langle n_{\mathrm{Cl}}\rangle-Z_{\mathrm{Cl}}\ , \quad (8)$$

$$\rho_2=\langle n_{\mathrm{Pt^{II}}}\rangle-Z_{\mathrm{Pt}}\ , \quad (9)$$

$$\rho_3=\langle n_{\mathrm{Pt^{IV}}}\rangle-Z_{\mathrm{Pt}}\ , \quad (10)$$

where $\langle\cdots\rangle$ denotes the expectation value over the mean-field approximation (MFA) solution—e.g., $\langle n_{\mathrm{Pt}}\rangle$ means the expectation value of electron charge on a Pt site: $n_{\mathrm{Cl}}=\langle c_{\mathrm{Cl}}^{\dagger}c_{\mathrm{Cl}}\rangle$, etc.

The parameters μ and ν in the ion-ion attraction term, Eq. (4), are determined by fitting stoichiometric ground-state properties. In this case, Eq. (5) yields

$$\nu=\frac{\ln[(t_1-\rho_1\rho_2V_c/a_l^2)/(t_2-\rho_1\rho_3V_c/a_s^2)]}{\ln(a_s/a_l)}-1\ , \quad (11)$$

$$\mu=\frac{(t_1-\rho_1\rho_2V_c/a_l^2)}{a_l^{\nu+1}}. \quad (12)$$

Now let us investigate the consequences of the combined interactions of Eqs. (3) and (4). *First*, they redefine the on-site energy, e_0. The effective energy splitting $(2\bar{e}_0)$ between the M and X bands in the valence localized limit (i.e., $t_0\sim\alpha\sim 0$) for the undimerized chain can be easily derived from the Hamiltonian (1) as

$$2\bar{e}_0\simeq 2e_0+2V_c\frac{(Z_{\mathrm{Pt}}-Z_{\mathrm{Cl}}+n_{\mathrm{Cl}}-n_{\mathrm{Pt}})}{a}. \quad (13)$$

Replacing $Z_{\mathrm{Pt}}=4$, $Z_{\mathrm{Cl}}=1$, $n_{\mathrm{Cl}}=2$, and $n_{\mathrm{Pt}}=1$, we find that in order to have a physically reasonable (4–6 eV) location of the Pt band above the Cl band, we need to choose a relatively large *negative* e_0 for the value of V_c chosen in Table II: Only $\bar{e}_0$ is physically meaningful. Note that this M/X band separation is slightly different from $2e_0^{\mathrm{eff}}$ defined in the Appendix.

Second, we can define a bare *intra*site electron-lattice coupling strength (analogous to β in Ref. 4) by taking the first derivative of the energy contribution (3) with respect to x_i and identify the coefficient in front of the electron density operator n_i (see the Appendix). In this sense, Eq. (3) defines an *anharmonic* extension of intra-site electron-lattice coupling.

Third, the bare nearest-neighbor elastic constant, K_{MX}^{bare} (i.e., with renormalization by electron-phonon or electron-electron interactions), is given by taking the second derivative of the energy terms (3) and (4) with respect to x_i, yielding

$$K_{MX}^{\mathrm{bare}}=2V_c\frac{(n_i-Z_i)(n_{i+1}-Z_{i+1})}{(x_{i+1}-x_i+a)^3}+\frac{\mu\nu(\nu+1)}{(x_{i+1}-x_i+a)^{\nu+2}}\ . \quad (14)$$

We see that the combined electrostatic and Coulomb interactions, (3) and (4), provide an effective bare elastic constant, but again *anharmonically* extended with respect to K_{MX} introduced in Ref. 4.

Having determined the mean-field lattice, charge and spin distributions self-consistently (for either homogeneous or inhomogeneous cases, Secs. III and IV), linear fluctuations around these mean-field states can then be calculated numerically and electronic optical absorption, infrared and Raman phonon spectra, and other response functions calculated at a random-phase-approximation (RPA) level—see Refs. 4 and 14 for details. In particular, for polaron, soliton, and exciton self-trapped defects there are local "shape oscillations" which give rise to electronic absorption within the IVCT gap, and corre-

sponding infrared and Raman modes shifted in frequency relative to those of the homogeneous chain.

III. STOICHIOMETRIC GROUND STATES AND THE TEMPLATE EFFECT

In this section we consider stoichiometric (i.e., homogeneous) ground states. Parameter values (t_0, α, e_0, U_M, U_X, V_c) for the Hamiltonian (1) are chosen by fitting to experimental data as follows. We first diagonalize the Hamiltonian (1) and then insert the obtained electronic spectrum into the energy minimization equation (5) to obtain the corresponding lattice positions. After iterating these steps to convergence, we evaluate the mean-field IVCT energy gap and dimerization magnitude. We then use the RPA to compute the Raman phonon frequency. We fit these three theoretical predictions to the available experimental data[2] by a least squares fitting method. Note that μ and ν are determined from Eqs. (11) and (12). Also we have taken a K_{MM} value suggested from experimental literature[12] and consistent with our previous model parametrization[4]. In addition we constrain the separation of M and X bands to the range of 4–6 eV, as explained in Sec. II. Since we have more model parameters than input experimental data, and the set of relationships is nonlinear, we do not expect that the parameters set is unique. Final determination will depend on additional experimental data becoming available (charge-densities, infrared modes, ESR, etc.). However, the parameters are chosen with physically reasonable values to satisfy the above constraints, and are capable of explaining systematic variations for self-trapped defects, as shown in Sec. IV.

We have used the above procedure to investigate the stoichiometric ground-state properties of two PtCl materials, $[Pt_2(en)_4Cl_2](ClO_4)_4$ and $[Pt_2(chxn)_4Cl_2]Cl_4$. These two materials differ only by ligand [en (ethylenediamine) and chxn (cyclohexanediamine)] and a counterion. As pointed out by Scott *et al.*,[13] different ligands and counterions bring about major changes in ground-state properties, primarily because of the change of the average lattice constant a. Table I shows the experimental data available for their stoichiometric ground-state properties: Peierls-distortion strength (defined as the ratio of the short to long Pt-Cl bond length), IVCT energy gap, and Raman frequency ν_1. These properties exhibit a consistent trend as the Peierls-distortion strength weakens from the former to the latter material. Using the approach described above to fit the experimental stoichiometric ground-state properties shown in Table I, we found two sets of parameters for these two materials, as summarized in Table II.

From Table II, the template effect is very clear. The fact that both t_0 and α for $[Pt_2(en)_4Cl_2](ClO_4)_4$ are very small and the Coulomb V_c coefficient is large, suggests that indeed it is a very valence-localized, strong charge-density-wave (CDW) material. On the other hand, for $[Pt_2(chxn)_4Cl_2]Cl_4$, both t_0 and α are larger and V_c is smaller. This indicates that the latter is a weaker CDW, less valence-localized material, as anticipated. The same trend is clear from the charge distributions we calculate in our model with the parameter sets in Table II. The stoichiometric charge distributions are 1.98, 1.90 (Pt^{II}); 0.04, 0.40 (Pt^{IV}); 1.99, 1.85 (Cl), for the localized and more delocalized cases above, respectively.

IV. DEFECT STATES

In this section, we discuss the self-trapped defect states formed by adding electrons or holes into $[Pt_2(en)_4Cl_2](ClO_4)_4$ and adding relaxation of electronic and lattice fields. Removing or adding an extra electron from a stoichiometric PtX chain forms a hole or electron polaron, respectively. Exciting an electron from the top of the filled majority-Pt valence band into the bottom of the empty conduction band and allowing relaxation can result in a self-trapped exciton, either singlet or triplet depending on spin configuration. Solitons are formed in an MX chain of length $4n+2$, where n is an integer. They can be neutral or negatively or positively charged. We use the *same* procedure described earlier to evaluate lattice distribution, electronic absorption, and phonon properties following from the Hamiltonian (1), with the *same* model parameters as for the homogeneous stoichiometric chain (Sec. III). Depending upon the choice of material, the locally changed charge-density associated with defect states may or may not extend over a long segment of the chain. Since PtCl is a very localized CDW material, any self-trapped defect is also expected to be confined within very few PtCl units. Due to the locally changed charge-density and Pt-Cl bond lengths, the elastic constant K_{MX}^{bare} [Eq. (14)] also changes locally, resulting in strong changes in Raman local mode frequencies.

We note one further interesting feature. Without allowing any *buckling*, the calculated electron polaron Raman mode would have higher frequency than that for the hole polaron. This is because removing a charge (tend-

TABLE I. Experimental data and theoretical prediction (in parentheses), using parameters in Table II, for the ground-state properties of $[Pt_2(en)_4Cl_2](ClO_4)_4$ (*a*) and $[Pt_2(chxn)_4Cl_2]Cl_4$ (*b*). The experimental long and short Pt-Cl bond lengths are input to the theory. The Peierls-distortion strength ξ is defined as the ratio of short and long Pt-Cl bond lengths (therefore, smaller ξ means stronger Peierls distortion).

	Pt^{IV}–Cl (Å)	Pt^{II}–Cl (Å)	CDW strength	IVCT (eV)	Raman frequency (cm^{-1})
(*a*)	2.327	3.101	0.75	2.5 (2.50)	311 (307)
(*b*)	2.324	2.834	0.82	1.6 (1.58)	280 (279.6)

TABLE II. Parameter sets for $[Pt_2(en)_4Cl_2](ClO_4)_4$ (a) and $[Pt_2(chxn)_4Cl_2]Cl_4$ (b). Values of μ and ν are deduced from Eqs. (11) and (12). $K_y = 0.55$ eV/Å is used to fit electron polaron Raman data for $[Pt_2(en)_4Cl_2](ClO_4)_4$ in Table III.

	t_0 (eV)	e_0 (eV)	α (eV/Å)	U_M (eV)	U_X	V_c (eV Å)	K_{MM} (eV/Å^2)	ν	μ
(a)	0.06	-17.79	0.0187	0.343	0.0	13.26	2.5	3.41	119.3
(b)	1.6	-8.6	1.8	0.2	0.4	7.82	2.5	4.57	148.8

ing to contract Pt^{II}-Cl bonds) will soften the local elastic constant more than adding one (tending to expand the Pt^{IV}-Cl bonds) will. However, if we allow the Cl atoms on and near the electron polaron center to slightly buckle out of the chain, we reduce the electron polaron Raman frequency below the hole polaron's, consistent with experiment. Such buckling is physically reasonable for an *electron* polaron.[14]

To model buckling, we introduced a further parameter into the Hamiltonian (1), namely a (harmonic) elastic constant, K_y (see Table II) associated with the movement of Cl in the direction perpendicular to the chain. K_y characterizes effects associated with the ligand and counterion environment.

The self-consistent equation (5) needs to be modified in the case of buckling, and one more self-consistent equation is needed in the y direction. The set of coupled equations are then

$$\frac{\mu\nu(x_{i+1}-x_i+a)}{R_{i,i+1}^{\nu+2}}+V_c\frac{(n_i-Z_i)(n_{i+1}-Z_{i+1})(x_{i+1}-x_i+a)}{R_{i,i+1}^{3}}-2\alpha\langle c_{i+1}^{\dagger}c_i\rangle$$

$$-\frac{\mu\nu(x_i-x_{i-1}+a)}{R_{i,i-1}^{\nu+2}}-V_c\frac{(n_i-Z_i)(n_{i-1}-Z_{i-1})(x_i-x_{i-1}+a)}{R_{i,i-1}^{3}}+2\alpha\langle c_i^{\dagger}c_{i-1}\rangle+K_{i-1}(x_i-x_{i-2})-K_{i+1}(x_{i+2}-x_i)=0\ , \tag{15}$$

$$\frac{\mu\nu y_{i+1}}{R_{i,i+1}^{\nu+2}}+V_c\frac{(n_i-Z_i)(n_{i+1}-Z_{i+1})y_{i+1}}{R_{i,i+1}^{3}}+K_y(y_i-y_{i+1})-\frac{\mu\nu y_i}{R_{i,i-1}^{\nu+2}}-V_c\frac{(n_i-Z_i)(n_{i-1}-Z_{i-1})y_i}{R_{i,i-1}^{3}}+K_y(y_i-y_{i-1})=0\ . \tag{16}$$

Buckling of course costs elastic energy. However, more energy is gained by suppressing an expansion in the chain direction which we find to occur if buckling is not allowed. The buckling occurs only if K_y is small enough. We found that there is a threshold value for K_y (in the case of $[Pt_2(en)_4Cl_2](ClO_4)_4$ which we studied, this value is about 0.7 eV/Å^2), above which there would be no buckling at all. This effect may be relevant for pressure studies. The threshold value depends upon the type of defect. For example, for an electron bipolaron it is higher than that for an electron polaron. We also note that we find no buckling for exciton states (triplet or singlet). The value of K_y we used to fit the experimental $[Pt_2(en)_4Cl_2](ClO_4)_4$ electron polaron Raman frequency is 0.55 eV/Å^2 (Table II). The buckling found for the electron bipolaron is of course greater than for the electron polaron using the same value of K_y.

In our calculation, we can also *constrain* an electron-doped chain to be unbuckled. This results in the chain being more extended in the chain direction than the buckled chain, leading to a higher total energy (see discussion below). Figure 3 contrasts the difference of lattice configurations around the center of an electron polaron for buckled (a) and unbuckled (b) chains.

Table III summarizes our calculations[4,11] of the electronic optical absorption and Raman phonon frequencies for various self-trapped defects—electron and hole polarons and bipolarons, singlet and triplet excitons, neu-

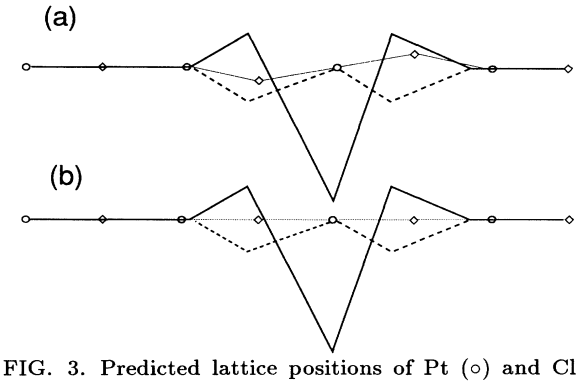

FIG. 3. Predicted lattice positions of Pt (○) and Cl (◇) atoms, excess charge density (solid line), and excess spin density (dashed line) near an electron polaron for buckled (a) and unbuckled (b) chains in $[Pt_2(en)_4Cl_2](ClO_4)_4$. Buckling out of the chain in (a) is 0.06 Å , but exaggerated here approximately three times. The unbuckled chain in (b) is more expanded ($\sim$ 0.005 Å) than the buckled chain in (a).

TABLE III. Characteristic Raman phonon frequency, electronic optical absorption peak energies for electron-hole polaron, electron-hole bipolaron, singlet-triplet excitons, neutral-positive-negative solitons. Parameters are taken from Table II.

Type of defect	Raman frequency	Optical absorption peak energy	Buckling
Electron polaron P^-	263 cm^{-1}	0.6, 2.08, 2.34 eV	Yes, 0.06 Å
Hole polaron P^+	288 cm^{-1}	0.6, 1.75, 2.38 eV	No
Electron bipolaron B^{--}	260 cm^{-1}	1.72, 2.15 eV	Yes, 0.1 Å
Hole bipolaron B^{++}	290 cm^{-1}	1.78, 2.22 eV	No
Singlet exciton	285, 252 cm^{-1}	0.55, 1.55, 2.14 eV	No
Triplet exciton	284, 257 cm^{-1}	0.67, 1.6, 2.38 eV	No
Neutral soliton S^0	282 cm^{-1}	2.25 eV	Yes, 0.09 Å
Positive soliton S^+	290 cm^{-1}	2.15 eV	No
Negative soliton S^-	276 cm^{-1}	1.85 eV	Yes, 0.11 Å

tral and charged solitons. Figures 4–7 show their corresponding predicted optical absorptions. We restrict ourselves to the buckling of Cl atoms only on or near the center of the electron defect in the calculation reported in Table III.

We emphasize several significant points from our calculations.

(i) The optical absorption peaks below the IVCT gap (2.5 eV) of a uniform chain shown in Table III and Figs. 4–7 are associated with specific intragap local defect states.

(ii) We notice that the Raman frequency for a bipolaron is not very different from the corresponding polaron. This is due to compensating changes in charge and lattice relaxation in Eq. (14), and may make experimental differentiation subtle.

(iii) One direct consequence of PtCl being highly valence localized is that the electronic Pt band is very flat. This remains to be adequately tested by experiment. Optical absorption data suggest a conduction bandwidth of about 0.5 eV. However, the onset may easily arise from exciton or other defect absorption (Table III) as well as disorder and quantum lattice fluctuations.[15]

(iv) More experiments are needed to confirm our assignment of Raman modes for bipolarons and excitons. ESR measurement may provide important information in this direction.[8]

(v) We have calculated the energy difference between the buckled and unbuckled electron polaron, and found it to be of the order of 100 K. We can anticipate thermal mixing of the two configurations to be reflected in experiments above this characteristic temperature: tunneling between degenerate buckled states should occur at lower temperatures. Of course, states with (discrete) rotations of the buckled configuration around the chain axis can be expected, and must be included in a complete tunneling description.

Finally, we should point out that PtBr and PtI in the MX family may also be studied within the present model. However, we reiterate that in these much more

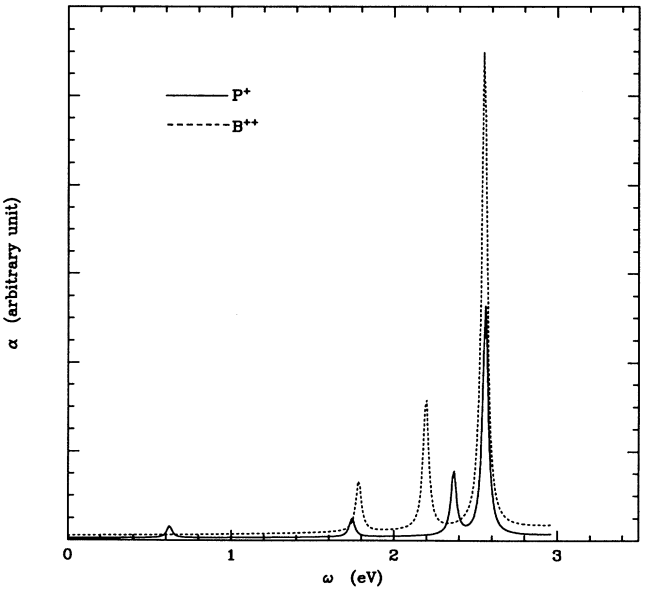

FIG. 4. Predicted optical absorption of hole polaron (P^+) and bipolaron (B^{++}) in $[Pt_2(en)_4Cl_2](ClO_4)_4$.

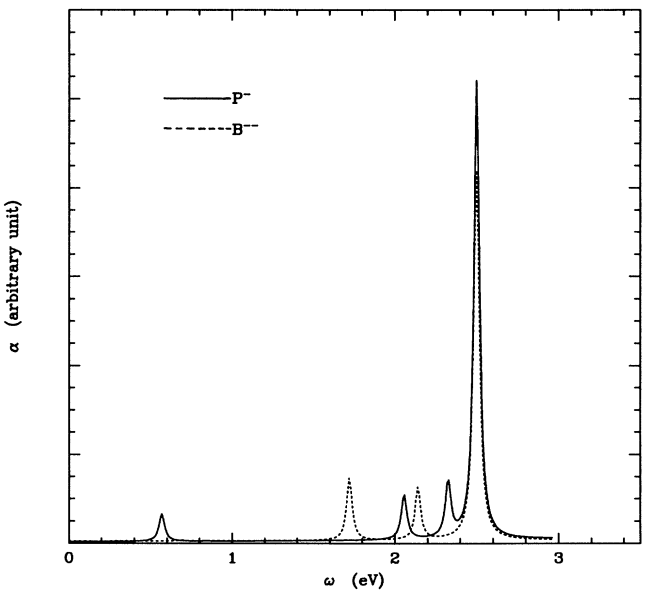

FIG. 5. Predicted optical absorption of the electron polaron (P^-) and bipolaron (B^{--}) in $[Pt_2(en)_4Cl_2](ClO_4)_4$.

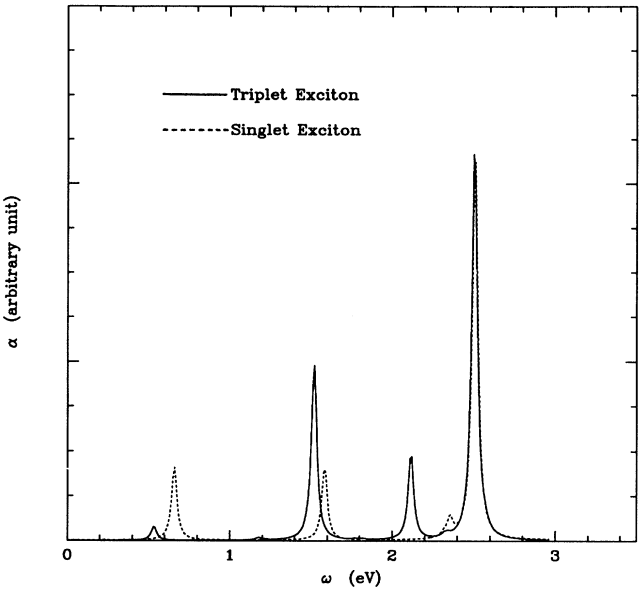

FIG. 6. Predicted optical absorption of triplet and singlet excitons in $[Pt_2(en)_4Cl_2](ClO_4)_4$.

delocalized CDW materials, the deviation from our previous linear Peierls-Hubbard model[4] is unimportant, as shown in the Appendix.

V. CONCLUSION

In this paper, we have discussed the Coulomb and electrostatic interactions in strongly valence-localized (e.g., PtCl) materials. In contrast to the linear elastic force and electron-lattice coupling in our previous extended Peierls-Hubbard model,[4] these interactions generate effective anharmonic elastic force and intrasite electron-lattice coupling. Two PtCl materials were compared, demonstrating a strong template effect. The various polaronic and self-trapped excitonic defect states were characterized by computing their corresponding optical absorptions and Raman frequencies, and good agreement with available experimental data was achieved—using the *same* model Hamiltonian and parameter values as for the corresponding stoichiometric material. We found that it is necessary for the electron polaron and bipolaron to buckle out of the chain direction to minimize energy, while no buckling for hole defects or excitons is predicted. This buckling accounts for the experimentally observed ordering of Raman phonon frequencies for electron and hole polarons. The explicit inclusion of Coulomb and electrostatic interactions is only essential for describing defect states in valence-localized materials, such as the PtCl compounds described in this manuscript. For valence-delocalized materials, our previous linear Peierls-Hubbard model is equivalent to the present one (see the Appendix).

In conclusion, we reiterate the essential need for an integrated synthesis—microscopic characterization—modeling strategy to achieve predictive control of strongly correlated electronic materials, such as those noted in Sec. I. The quantitative success of this strategy, for both stoichiometric ground and doped states in the class of MX compounds we have discussed here is very striking, and provides important guidance for novel electronic materials generally.

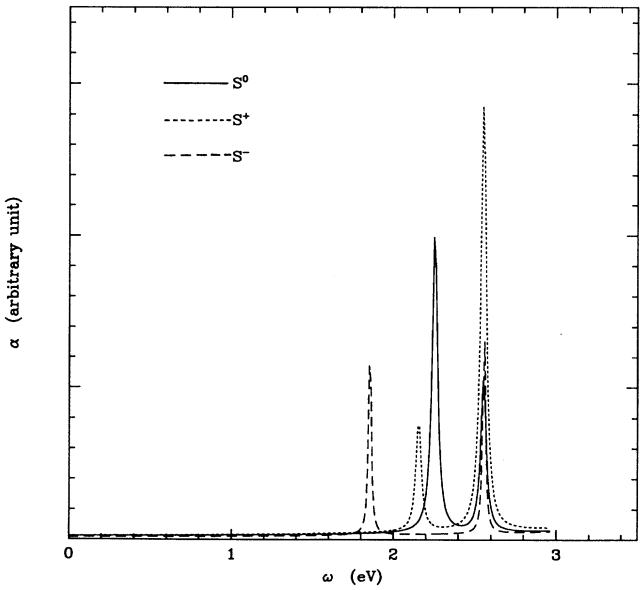

FIG. 7. Predicted optical absorption of neutral (S^0), positive (S^+), and negative (S^-) charged solitons in $[Pt_2(en)_4Cl_2](ClO_4)_4$.

ACKNOWLEDGMENTS

We thank J. T. Gammel, S. P. Love, B. L. Scott, and B. I. Swanson for extensive and illuminating discussions. The work at Los Alamos was supported by the U.S. Department of Energy.

APPENDIX: EXTENDED LIMIT OF THE MODEL HAMILTONIAN (1)

Here we show how the Hamiltonian (1) reduces to our previous harmonic Hamiltonian[4] in the case of weak dimerization and no chain buckling. This comparison is especially relevant to highly valence-delocalized MX materials such as PtI.

First, we expand the distance $R_{i,i+1}$ in the denominator of the Hamiltonian (1) around the average M-X bond length a up to second order:

$$\frac{1}{R^{\nu}_{i,i+1}} = \frac{1}{(a+\Delta_i)^{\nu}} \simeq \frac{1}{a^{\nu}} - \frac{\nu\Delta_i}{a^{\nu+1}} + \frac{\nu(\nu+1)\Delta_i^2}{a^{\nu+2}}. \quad \text{(A1)}$$

We define

$$A = Z_i Z_{i+1} - \langle c_i^{\dagger} c_i \rangle \langle c_{i+1}^{\dagger} c_{i+1} \rangle. \quad \text{(A2)}$$

In the homogeneous undimerized case, $A = 2$ is a constant independent of i. Our Coulomb and electrostatic terms for site i are thus given by

$$\frac{V_c A}{R_{i,i+1}} + \frac{\mu}{R^{\nu}_{i,i+1}} \simeq \text{const} - \Delta_i \left(\frac{V_c A}{a^2} + \frac{\nu\mu}{a^{\nu+1}} \right) + \frac{1}{2} \Delta_i^2 \left(\frac{2V_c A}{a^3} + \frac{\nu(\nu+1)\mu}{a^{\nu+2}} \right). \tag{A3}$$

The linear term with Δ_i is canceled when summing over i since

$$\sum_i \Delta_i = 0. \tag{A4}$$

The second order term in Δ_i in Eq. (A3) provides the elastic constant for an MX bond:

$$K_{i,i+1} = K_{MX} = \frac{2V_c A}{a^3} + \frac{\nu(\nu+1)\mu}{a^{\nu+2}}. \tag{A5}$$

This is a *harmonic* elastic constant, which is a limit of Eq. (14) for the undimerized case.

Now consider the electron-phonon interaction. Expanding the coefficient before the term $n_{i\sigma} = c^{\dagger}_{i,\sigma} c_{i,\sigma}$ in Eq. (1) up to the linear order, we have the following.

(i) If $i = M$ site,

$$-\frac{V_c Z_X}{(a+\Delta_i)} - \frac{V_c Z_X}{(a+\Delta_{i-1})} \simeq -\frac{2V_c Z_X}{a} + (\Delta_i + \Delta_{i-1}) \frac{V_c Z_X}{a^2}. \tag{A6}$$

(ii) If $i = X$ site,

$$-\frac{V_c Z_M}{(a+\Delta_i)} - \frac{V_c Z_M}{(a+\Delta_{i-1})} \simeq -\frac{2V_c Z_M}{a} + (\Delta_i + \Delta_{i-1}) \frac{V_c Z_M}{a^2}. \tag{A7}$$

Therefore, e_0 is renormalized as

$$2e_0^{\text{eff}} \simeq 2e_0 + \frac{2V_c(Z_M - Z_X)}{a}, \tag{A8}$$

and the on-site electron-phonon coupling is given by

$$\beta_M = \frac{V_c Z_X}{a^2}, \tag{A9}$$

$$\beta_X = \frac{V_c Z_M}{a^2}. \tag{A10}$$

Putting together Eqs. (A5) and (A8)–(A10), the reduced Hamiltonian now reads

$$H \simeq \sum_i -(t - \alpha\Delta_i)(c^{\dagger}_i c_{i+1} + c^{\dagger}_{i+1} c_i) + (-) i e_0' c^{\dagger}_i c_i - \sum_i \beta_i (\Delta_i + \Delta_{i-1}) c^{\dagger}_i c_i + \sum_i \frac{K_i}{2} \Delta_i^2 + \frac{M_i}{2} \dot{x}_i^2. \tag{A11}$$

This is precisely the same as our previous *harmonic* Hamiltonian.[4]

[1] M. B. Robin and P. Day, in *Advances in Inorganic Chemistry and Radiochemistry*, edited by H. J. Emeleus (Academic, New York, 1967), Vol. 10, p. 247; P. Day, in *Low Dimensional Cooperative Phenomena*, edited by H. J. Keller (Plenum, New York, 1974), p. 191; H. J. Keller, in *Extended Linear Chain Compounds*, edited by J. S. Miller (Plenum, New York, 1982), Vol. 1, p. 357; R. J. H. Clark, in *Advances in Infrared and Raman Spectroscopy*, edited by R. J. H. Clark and R. E. Hester (Wiley, New York, 1984), and references therein.

[2] R. J. Donohoe, S. A. Ekberg, C. D. Tait, and B. I. Swanson, Solid State Commun. **71**, 49 (1989); R. J. Donohoe, R. B. Dyer, and B. I. Swanson, *ibid.* **73**, 521 (1989); R. J. Donohoe, C. D. Tait, and B. I. Swanson, Chem. Mater. **2**, 315 (1990), R. J. Donohoe, L. A. Worl, B. I. Swanson, and A. Bulou, Synth. Met. **41-43**, 2749 (1991).

[3] S. P. Love, S. C. Huckett, T. M. Frankcom, S. A. Ekberg, and B. I. Swanson, Phys. Rev. B **47**, 11 107 (1993).

[4] J. T. Gammel, A. Saxena, I. Batistić, A. R. Bishop, and S. R. Phillpot, Phys. Rev. B **45**, 6408 (1992); S. M. Weber-Milbrodt *et al.*, *ibid.* **45**, 6438 (1992).

[5] X. Z. Huang, A. Saxena, A. R. Bishop, L. A. Worl, S. P. Love, and B. I. Swanson, Solid State Commun. **84**, 957 (1992).

[6] X. Z. Huang *et al.*, J. Phys. (to be published).

[7] L. A. Worl *et al.*, J. Phys.: Condens. Matter **4**, 10237 (1992).

[8] A. Saxena *et al.* (unpublished).

[9] C. Kittel, *Introduction to Solid State Physics*, 6th ed. (Wiley, New York, 1986).

[10] I. Batistić and A. R. Bishop, Phys. Rev. B **45**, 5282 (1992). We should note that intrinsic doping within this model induces local phonon modes only through the random-phase-approximation (RPA) renormalization.

[11] J. T. Gammel, R. J. Donohoe, A. R. Bishop, and B. I. Swanson, Phys. Rev. B **42**, 10 566 (1990).

[12] A. D. F. Bulou, R. J. Donohoe, and B. I. Swanson, J. Phys: Condens. Matter **3**, 1709 (1991).

[13] B. L. Scott *et al.*, Inorg. Chem. (to be published); H. Okamoto, K. Toriumi, T. Mitani, and M. Yamashita, Mol. Cryst. Liq. Cryst. **218**, 247 (1992).

[14] See, e.g., discussion of buckling by M. Suzuki and K. Nasu, Phys. Rev. B **45**, 1605 (1992).

[15] R. H. McKenzie and J. W. Wilkins, Phys. Rev. Lett. **69**, 1085 (1992).